AIAA-2003-0751
Investigation of Aerodynamic Scale Effects for a Generic Fighter Configuration in the National Transonic Facility (Invited)

W. G. Tomek, R. A. Wahls, L. R. Owens, A. B. Burner,
S. S. Graves, and J. M. Luckring
NASA Langley Research Center
Hampton, Virginia

41st AIAA Aerospace Sciences Meeting & Exhibit
6-9 January 2003
Reno, Nevada

INVESTIGATION OF AERODYNAMIC SCALE EFFECTS FOR A GENERIC FIGHTER CONFIGURATION IN THE NATIONAL TRANSONIC FACILITY

W. G. Tomek[1], R. A. Wahls[2], L. R. Owens[3] A. B. Burner[4], S. S. Graves[5], and J. M. Luckring[6]

Aerodynamics, Aerothermodynamics, and Acoustics Competency
NASA Langley Research Center
Hampton, Virginia

ABSTRACT

Two wind tunnel tests of a generic fighter configuration have been completed in the National Transonic Facility. The primary purpose of the tests was to assess Reynolds number scale effects on a thin-wing, fighter-type configuration up to full-scale flight conditions (that is, Reynolds numbers of the order of 60 million). The tests included longitudinal and lateral/directional studies at subsonic and transonic conditions across a range of Reynolds numbers from that available in conventional wind tunnels to flight conditions.

Results are presented for three Mach numbers (0.6, 0.8, and 0.9) and three configurations: 1) Fuselage / Wing, 2) Fuselage / Wing / Centerline Vertical Tail / Horizontal Tail, and 3) Fuselage / Wing / Trailing-Edge Extension / Twin Vertical Tails. Reynolds number effects on the lateral-directional aerodynamic characteristics are presented herein, along with longitudinal data demonstrating the effects of fixing the boundary layer transition location for low Reynolds number conditions. In addition, an improved model videogrammetry system and results are discussed.

INTRODUCTION

Ground-based experimentation at full-scale Reynolds numbers is now available through the use of cryogenic wind tunnels, such as the National Transonic Facility (NTF) at the NASA Langley Research Center. Some of the initial models tested in this facility were built to study the Reynolds number effects on transport aircraft. These models were composed of U.S. aircraft industry designed and fabricated wings mounted to a NASA supplied generic fuselage, denoted as Pathfinder I (refs. 1 and 2). A similar need was identified for studying fighter aircraft concepts. A sequence of fighter-class configurations were developed and denoted by NASA as Pathfinder II. Further general discussion of the Pathfinder II family of models can be found in references 1 – 3.

The objectives of the current wind tunnel investigation, utilizing the Pathfinder II fuselage with a McDonnell Douglas defined thin, fighter-type wing, were to study the effects of Reynolds number on a fighter-type configuration through model component build-up and with stability and control device deployment (ref. 4). The tests were conducted to provide a database of Reynolds number effects, up to full scale, which could be used to determine Reynolds number correlation trends, provide data for assessment of computational fluid dynamics (CFD) methods including turbulence modeling, and validate design and analysis methods.

[1]Aerospace Engineer, Research Facilities Branch, Member, AIAA

[2]Assistant Branch Head, Configuration Aerodynamic Branch, Associate Fellow, AIAA

[3]Aerospace Engineer, Flow Physics and Control Branch, Senior Member, AIAA

[4]Senior Research Scientist, Instrumentation Systems Development Branch, Associate Fellow, AIAA

[5]Research Engineer, Instrumentation Systems Development Branch, Member, AIAA

[6]Senior Research Engineer, Configuration Aerodynamics Branch, Associate Fellow, AIAA

This paper presents results from two wind tunnel tests conducted in the National Transonic Facility at the Langley Research Center. The initial wind tunnel test, conducted from November – December 1995, focused on the Reynolds number sensitivities of the aerodynamic characteristics at subsonic and transonic conditions for three distinct configurations. This test was conducted over a range of Reynolds numbers (based on the mac) from 5 million to 61 million and utilized the air mode as well as the cryogenic capability of the facility. The three major configurations tested were 1) a standard Fuselage / Wing (FW) configuration, 2) a Fuselage / Wing / Centerline Vertical Tail / Horizontal Tail (FWV1H) configuration, and 3) a Fuselage / Wing / Trailing-Edge Extension / Twin Vertical Tail (FWTV2) configuration. The second test, conducted from November – December 2002, utilized the NTF's air-mode only and supplemented the free transition data from the first test with fixed transition data at low Reynolds numbers. Additionally, the second test provided model deformation data not previously available.

NOMENCLATURE

AF	Axial force
AR	Aspect ratio
BL	Butt line
CI95	95% confidence interval
C_D	Drag coefficient
C_L	Lift coefficient
C_M	Pitching-moment coefficient referenced to 0.42 mac
Cl	Rolling-moment coefficient referenced to 0.42 mac
Cl_β	Rolling-moment derivative, per deg
Cn	Yawing-moment coefficient referenced to 0.42 mac
Cn_β	Directional stability derivative, per deg
CR	Root chord
CT	Tip chord
CY	Side-force coefficient
CY_β	Side-force derivative, per deg
c	Local chord length
E	Modulus of elasticity
FW	Fuselage / Wing configuration
FWV1H	Fuselage / Wing / Centerline Vertical Tail / Horizontal Tail configuration
FWTV2	Fuselage / Wing / Trailing-Edge Extension / Twin Vertical Tail configuration
LaRC	Langley Research Center
LE	Leading edge
M	Mach number
mac	Mean aerodynamic chord
MS	Model station
NF	Normal force
NTF	National Transonic Facility
P_T	Total pressure
PM	Pitching-moment
Q	Dynamic pressure
RM	Rolling-moment
Rn	Reynolds number based on mac
SF	Side force
Sref	Reference area
T_T	Total temperature
TE	Trailing-edge
TEX	Trailing-edge extension
VMD	Videogrammetric model deformation
YM	Yawing-moment
α	Angle of attack
β	Angle of sideslip
η	Non-dimensional semispan station

EXPERIMENTAL APPROACH

Facility Description

The NTF is a unique national facility (fig. 1) that enables testing of aircraft configurations at conditions ranging from subsonic to low supersonic speeds at Reynolds numbers up to full-scale flight values, depending on the aircraft type and size. The facility (fig. 2) is a fan-driven, closed-circuit, continuous-flow, pressurized wind tunnel capable of operating in either dry air at warm temperatures or nitrogen from warm to cryogenic temperatures. The test section is 8.2 ft by 8.2 ft in cross section and 25 ft in length. The test section floor and ceiling are slotted (6 percent open), and the sidewalls are solid. Freestream turbulence is damped by four screens and utilizes a 15:1 contraction ratio from the settling chamber to the test section. Fan noise effects are minimized by an acoustic treatment both upstream and downstream of the

fan. The NTF is capable of an absolute pressure range from 15 psi to 125 psi, a temperature range from −260°F to 130°F, a Mach number range from 0.2 to 1.2, and a maximum Reynolds number of 146×10^6 per ft at Mach 1. Further facility details can be found in reference 5.

Model Description

The Pathfinder II model was designed by McDonnell Douglas to assess a variety of configuration concepts and aerodynamic issues pertinent to maneuvering aircraft. The model, shown in figure 3, has the capability for testing numerous aerodynamic concepts including: two segment leading-edge flaps, trailing-edge flaps and ailerons, a trailing-edge extension (TEX) with a trailing-edge flap, and a wing tiperon. Only the TEX, un-flapped configuration was tested. The three configurations tested for the current investigation are sketched in figure 4. Figure 5a shows a planform drawing of the model with pertinent reference geometry denoted. The model has a delta wing with an aspect ratio of 1.946, a span of 20.802 inches, and a mean aerodynamic chord of 13.434 inches. The wing has a leading-edge sweep of 65 degrees with a trailing-edge sweep on the outboard panel of 35 degrees. The airfoil section is a NACA 65A004 at the root and a NACA 65A005 at the tip with a linear thickness distribution from root to tip. Figure 5b details the geometry of the respective empennage components. The reference area for the model is 1.544 square feet.

The model was designed and constructed specifically for testing in the cryogenic, pressurized conditions of the NTF where dynamic pressures up to approximately 2300 psf were required for this investigation. The model was mounted in the NTF test section on a straight sting. The sting mounted to a stub sting which in turn mounted to the facility arc sector resulting in a model angle of attack range for the tests from −2 to 18 degrees. Pertinent model geometry as compared to the NTF test section geometry is shown in table 1. The model was relatively small in comparison to typical NTF transport or high-speed research models.

The model was instrumented with 43 pressure ports on the wing upper surface and 18 on the wing lower surface. Additionally, there were 22 upper surface pressure ports along the fuselage centerline (aft of nose) and slightly off-center on the aft fuselage. Data was collected from all available pressure ports on the model for the initial test of the model, but was limited to the baseline configuration (FW). The follow-on entry included surface pressure measurements for the baseline configuration as well as the twin-tail configuration (FWTV2). No pressure data analysis is presented herein.

Instrumentation

Aerodynamic force and moment data were obtained with an internal, unheated, six-component strain gauge balance. Design loads for the NTF 104B balance were: NF=3400 lbs, AF=300 lbs, PM=10,000 in-lbs, RM=5000 in-lbs, YM=5000 in-lbs, and SF=1000 lbs. The quoted accuracy from the calibration of the balance was less than or equal to 0.35 % of full-scale load for each balance component.

An internal, heated, single-axis, on-board accelerometer package was used to measure the model angle of attack for all zero sideslip conditions. The accelerometer package had a quoted accuracy, under smooth operating tunnel conditions, of ±0.01 degrees (ref. 6). For all sideslip conditions, facility arc sector measured pitch and roll angles plus calibrated sting bending were used to determine the model angle of attack and sideslip.

Model pressure measurements from both the wing and fuselage of the model were obtained, for the earlier wind tunnel test, using two 48-port, 30-psid, onboard, heated, electronically scanned pressure (ESP) transducers with a quoted accuracy of ±0.2 % of full-scale pressure range. The most recent test also included surface pressure measurements, but was limited to the wing. A 30-psid range, 64-port ESP module was used for this portion of the investigation. The body cavity pressure was measured at two locations inside the fuselage cavity with a heated, 2.5-psid ESP module located in the facility arc sector.

An exterior videogrammetry instrumentation system was also utilized for the second entry of the model. This system allowed the evaluation of wing twist and displacement measurements along three span stations of the wing. This system will be detailed in a follow-on section describing static aeroelastic effects.

The primary measured flow variables included both the total and static pressures and

the total temperature. Mach number, Reynolds number, and dynamic pressure were calculated from these measured parameters. A complete description of these measurements and subsequent calculations is given in reference 7.

Data Reduction and Corrections

Information on the various instrumentation devices, the data acquisition and control computers, and the data reduction algorithms for the different measurement systems is provided in reference 7. Standard balance, angle-of-attack, and tunnel parameter corrections have been applied. Note that the use of unheated balances in the cryogenic environment requires additional attention towards temperature compensation. The temperature compensation methods are designed to correct balance output due to thermal loads. Body cavity pressure corrections were applied based on the measurements described previously and were used to correct drag. The angle of attack was corrected for flow angularity (upflow) by measurement of both upright and inverted model force data for a given configuration and flow condition. Wall and model support interference effects have not been accounted for in the data; wall effects are assumed minimal due to the model size relative to the test section (see table 1).

Test Conditions

The test program was set-up to evaluate the effect of full-scale Reynolds numbers and produce an aerodynamic database applicable to thin-wing, fighter-type configurations. The NTF allows testing across a wide range of Reynolds numbers from that available in conventional wind tunnels to near flight conditions at subsonic and transonic Mach numbers. The Reynolds numbers chosen for the test matched full-scale conditions at selected altitudes of 20,000, 30,000, and 40,000 feet, representative of operational fighter aircraft altitudes. Tests of the Pathfinder II model spanned Reynolds numbers from 5 million to 60.9 million at Mach numbers 0.6, 0.8, and 0.9. Representative test points for Mach 0.9 are shown in figure 6. Data were obtained at several total temperature conditions requiring both air and nitrogen mode operations. Included in this envelope is a representative extended air mode test condition (condition 7). This condition represents an improvement of approximately 50% in the cooling capacity of the facility in air-mode operations. This capacity was obtained with the enhancements to the NTF cooling coil completed recently. Data were obtained over an angle-of-attack range from –2 to 18 degrees.

The initial configuration, during the first model entry, was tested to acquire force and model pressure data simultaneously. In an attempt to relieve any possible fouling or any thermally induced loads from the pressure tubing bridging the balance, the pressure tubes were cut and removed after a set of pressure data was acquired on the initial Fuselage / Wing configuration. The configuration was then re-tested for only force and moment data. Hence, there is force and moment data for all three configurations available, but only pressure data available for the Fuselage / Wing configuration for the high Reynolds number conditions. For the second entry of the model, there was an improved technique utilized to collect both force and moment data simultaneously with the surface pressure data. Also, since there was only one temperature condition for this model entry, the likelihood of any significant fouling from the pressure tubing or instrumentation was minimized.

Boundary-Layer Transition

A basic strategy used at the NTF includes testing at high Reynolds number conditions with free transition. The high Reynolds number test condition typically corresponds to a design flight condition. To anchor the NTF data to low Reynolds number data obtained in a conventional wind tunnel, the NTF model is usually tested at a matching low Reynolds number condition with the boundary-layer tripping (forced/fixed transition) strategy used in a conventional wind tunnel. For the initial investigation, no tripping of the boundary layer was utilized for any test condition (Mach, Reynolds number) since the test focused on the high Reynolds number data evaluation. However, the follow-on entry focused on a systematic boundary-layer transition evaluation at several low Reynolds numbers. The results obtained from this study will be discussed in succeeding sections.

RESULTS & DISCUSSION

The purpose of this paper is to document the Reynolds number sensitivities of lateral-directional aerodynamic characteristics

for a generic fighter configuration at subsonic and transonic conditions. Another objective is the demonstration of the effects of fixing boundary layer transition for low Reynolds number conditions on the longitudinal aerodynamic characteristics of the configurations. The three configurations investigated were a baseline Fuselage / Wing assembly (FW), a configuration with a centerline vertical tail and a horizontal tail (FWV1H), and a twin vertical tail configuration with a trailing-edge extension (FWTV2). Figure 7 shows representative data for the three configurations at a representative Mach number of 0.6 at a medium Reynolds number of 22 million and is provided to indicate the basic aerodynamic characteristics of the configurations. The lift-curve slopes for the three configurations display somewhat comparable characteristics. They include the effect of the formation of the leading-edge vortex on the wing at an angle of attack of about 4 degrees and corresponding drag characteristics. The pitching moment data contrasts the stable characteristics of the horizontal tail configuration with the unstable baseline and twin vertical tail configurations at angles of attack greater than about 8 degrees. Figure 8 shows representative lateral-directional data for a low Reynolds number condition (Rn = 5 million). This figure shows the variation of the lateral-directional coefficients with sideslip angle at a constant angle of attack of approximately 6 degrees and a Mach number of 0.6. Stable directional characteristics (Cn) for the tailed configurations for the entire sideslip range are seen in the figure as well as an unstable character of the baseline (FW) configuration. In addition, similar unstable trends are noted for the rolling moment as a function of sideslip for all three configurations. The data, as acquired at varying Reynolds numbers, included the combined effects of aeroelastic deformation and Reynolds number effects because the conditions at which the data were acquired were at different dynamic pressure levels in general; further discussion will address the aeroelastic effects.

Repeatability

The repeatability of the force and moment data from the Pathfinder II model was analyzed within each test, and over the long-term (7 years), between the two tests. Repeat runs were not conducted for every configuration or for all Mach numbers, but were scattered throughout each test. The analysis for the available repeat runs was conducted using the methodology as described in reference 8. The analysis consists of statistical determination of the mean value of the selected coefficients from repeated runs, a curve fit of the data using a 2nd order polynomial, and a determination of the residual of the individual data points from the curve fit data. Confidence intervals are determined and are defined as the bounds about an estimated mean that encompasses the true mean value with a probability of 95 % confidence.

Short-term repeatability for the first test is reported in reference 9 for low to high Reynolds number conditions (air and cryogenic operations). The results indicated excellent repeatability for attached flow conditions, with some degradation where separated flow dominates; regardless, the repeatability is comparable to the quoted balance accuracy. Short-term repeatability for the low Reynolds number conditions in the second test was comparable to similar conditions in the first test.

Long-term repeatability was not assessed in reference 9, as the second test had not been executed. A representative long-term repeatability analysis is shown in figure 9 for the longitudinal coefficients at Mach 0.6 and Rn = 5 million. The drag data shows a distinct effect of test (Test 77 vs. Test 140). There is a block effect, or offset, between the two sets of data, of about 2 counts of drag for the attached flow regime. There is a greater offset, of up to 6 counts, for the separated flow angles of attacks. The lift and pitching-moment data indicate excellent long-term repeatability. The confidence intervals shown in the figure assume a random distribution of data about a mean, but for the long-term analysis of these model entries, especially for drag, there is a distinct bias present, so the calculated confidence intervals are not technically correct.

A representative long-term repeatability analysis for the lateral-directional coefficients is shown in figure 10. A residual analysis was not available for this constant angle of attack, varying sideslip set of data. However, the data are very repeatable, and compare favorably to the quoted balance accuracy.

Static Aeroelastic Effects

The investigation of aerodynamic effects

on a model in a variable-pressure facility, such as the NTF, should take into account the possible aeroelastic effects. These effects could mask the other aerodynamic effects, such as Reynolds number effects, which are being studied. Since the NTF is capable of controlling Mach number, dynamic pressure, and temperature independently, the desired test plan would be to test at comparable dynamic pressures, or more specifically, comparable dynamic pressures divided by modulus of elasticity (Q/E) values, over the range of Mach and Reynolds number of interest. However, based on limitations on the strength of the model material, tunnel capability limitations, or nitrogen usage rates, the test plan is normally compromised, and the data from the test, if required, are "normalized" to provide similar wing shape comparisons.

Data for this particular model were taken at two different dynamic pressure levels at the same Reynolds number (Rn=22 million) as described in reference 9. Aeroelastic effects on the longitudinal aerodynamic coefficients were detectable, even for this low aspect ratio configuration, but were generally small. It was decided not to adjust data for these effects in the analysis. Wing twist videogrammetric measurements (reference 10) under load acquired in the second test of this model have also added to understanding of these effects and are described below.

Wing Deformation System and Measurements

The videogrammetric model deformation (VMD) single-camera single-view technique (ref. 11) was used to measure the change in wing twist due to aerodynamic loading. This was the first test at the NTF in which a recently developed and enhanced model deformation measurement system (ref. 12) was used as the primary system for the measurement of wing deformation. (However, the new system was recently successfully used during a transport test as a primary measurement system to obtain first-of-their-kind horizontal stabilizer deformation, installation repeatability, and aft-body bending due to aerodynamic loading.) This new system was designed to enable significant elements of intelligence to be incorporated into the measurement system. These elements of intelligence are essential to take model deformation measurements to the next level of robustness, accuracy, adaptability, and ease of use for facility operations personnel. The system incorporates a windows-based operating system that is familiar to most, is more user-friendly, and has a more flexible and robust tunnel data acquisition system interface. The new system is also optimized to use a progressive scan video-rate charge coupled device camera that has twice the vertical resolution of cameras used in the past. The new system is better able to accommodate variations in image quality by enabling the automatic adjustment of image processing parameters as a function of the model pitch angle and Mach number. Code to automatically reject outliers during in-situ calibration was also implemented and successfully tested for the first time during this test. A noteworthy accomplishment during this test was that the new deformation measurement system was also able to operate simultaneously with a new focus schlieren flow visualization system, recently installed and undergoing evaluation testing at the NTF, without procedural changes and without interference to either system.

A much faster peripheral component interconnect-based frame grabber board coupled with optimized coding enables 60 images per data point to be acquired and analyzed without any additional delay to the normal data taking rate at the NTF. Only 8 images per data point were typically analyzed during transport testing with the older system due to its inability to keep up with the data-taking rate at faster image analysis rates. The analysis of 60 images versus 8 images is not a major consideration for static laboratory or wind-off testing. However, definite improvements are seen as more images are analyzed for cases in which the dynamic motion itself is of interest or as one approaches higher model pitch angles near onset of buffet. The analysis of more images per data point is also a help during cryogenic testing, even for wind-off (or near wind-off) reference runs used for in-situ calibration since thermal shadowgraph effects can cause significantly more image plane jitter than during near-ambient testing. In addition the precision index for mean data is improved by a factor of 2.7 when using 60 images instead of 8.

This was the first test at the NTF in which deformation measurements were made on a fighter-model configuration. The short span

of this model, compared to normal transports tested at the NTF, enabled the data camera to view the entire right wing (which was the wing closest to the camera) without viewing from the opposite side of the test section and looking across the fuselage, as is commonly done for transports. The advantage of viewing the wing closest to the camera is that target pairs near the wing tip will experience the most magnification instead of the least compared to more inboard targets. This helps in two ways. First, since target diameter near the tip is limited by chord length and the requirement for the targets to be sufficiently separated, the target image diameter will be significantly larger when viewing the tip when it is closest to the camera. In previous transport tests the image diameter of targets near the wing tip were typically smaller than necessary for optimum accuracy due to chord length limitations. Secondly, the separation of targets near the tip is also greater on the image plane when the tip is closest to the camera. A fundamental accuracy consideration for angle measurements is the fraction of the image plane occupied by the two targets used to calculate angles. Thus the increased image plane separation of target pairs due to increased magnification improves the accuracy of angle measurements.

Pairs of optical polished-paint targets (ref. 11) were placed on the right wing at 3 normalized semispan locations, η, equal to 0.328, 0.665, and 0.935 (figure 11). An unprocessed image from the data camera during testing is shown in figure 12 to illustrate the very high contrast. The glint on the leading edge of the right wing (visible at the middle-right of figure 12) did not interfere with automated image processing utilized to find image coordinates of the optical targets. The relatively short semispan of this model compared to transports normally tested at the NTF limited the number of spanwise measurement locations. For transports tested at the NTF, it is common to measure 5 semispan locations as well as body targets (which are used as references). The spacing of the targets at the 3 semispan locations of the fighter model from inboard to outboard were 7.55, 4.92, and 1.24 inches. The diameter of the targets was 0.5 inch. The measured thickness of all six targets was 0.5 mil or less (0.0005 inch). The measured surface roughness of all targets was less than 10 μinch. An additional target was applied to the right wing vertical twin tail component at the η = 0.328 location to enable measurements for the vertical twin tail configuration when that part was placed on the model for a configuration change.

Wind-off reference polars (both before and after a run series) are used for final system angle calibration based on the primary model angular measurement system, which for this test was a precision servo-accelerometer located on the arc sector. Corrected angular data from the most inboard pair of targets located at η = 0.328 were subtracted from the more outboard locations to partially account for sting-bending and potential common-to-all-stations angular measurement bias errors of the VMD technique. Thus the deformation at the thick (and reasonably rigid) most inboard station (η = 0.328) is taken to be identically zero. The angular calibration at each semispan location consists of a curve fit of corrected angle (based on the primary model measurement system) versus uncorrected optically measured angle. Polynomial curve fits have been used during previous tests to partially smooth random fluctuations during calibration runs, particularly for cryogenic operation. The improvements in the measurement system noted above have led to better repeatability between calibration runs made before and after a run series. Thus an investigation with improved curve fitting methods to replace the standard polynomial fits in order to more accurately represent the variation in calibration data is warranted. Figures 13 and 14 show data obtained at η = 0.935 after correction with calibration curve fitting using a 5^{th} order least squares polynomial compared to data corrected with interpolation using a piecewise cubic Hermite. The polynomial fits were obtained from a single fit at each semispan station to 2 wind-off calibration runs that bracket the flow runs. The piecewise interpolation was obtained on a calibration data set consisting of the mean of the x and y values (uncorrected and corrected angles) of the data from the 2 calibration runs. The data consists of 2 repeat runs at Mach 0.6 and a dynamic pressure equal to 589 psf and 2 repeat runs at Mach 0.9 and a dynamic pressure equal to 1560 psf over an angle of attack range of –2° to 17°. Piecewise cubic Hermite interpolation (with extrapolation if necessary) yields calibration fits similar to piecewise linear interpolation, but without abrupt

slope changes at the nodes. Note that the nonlinear structure present in figure 13 is reduced somewhat in figure 14. Similar improvements were noted at other conditions as well. Piecewise cubic interpolation was used for the remaining deformation data plots and is currently being evaluated for its suitability in future testing.

Figures 15 through 18 show variations in model geometry for 3 configurations consisting of fuselage/wing, single horizontal and vertical tail, and twin vertical tails. The conditions for the data plots presented are Mach 0.6 at dynamic pressures of 589 and 1415 psf and Mach 0.9 at dynamic pressures of 797 and 1560 psf. The corrected data for each configuration is taken from the means of 2 repeat runs, in both angle of attack and Δtwist. Thus a single symbol is used to represent mean data from 2 runs for each configuration at η = 0.935. The results from 12 run pairs (24 total runs) presented in the 4 plots indicate that variations in model geometry due to aerodynamic loading are relatively independent of configuration. The variation in the change in model geometry for the 3 configurations are only slightly more that the repeatability of back-to-back measurements, except possibly for the higher angles of attack. The maximum flow induced twist of 0.9° occurs at the outboard station at the largest dynamic pressure of 1560 psf. The wing is essentially undeformed at approximately 2°. The deformation data at alpha = –2° and 10° of figures 15 – 18 for the 3 configurations are plotted in figure 19 versus dynamic pressure. Linear least square fits to the data at the 2 angles of attack are superimposed to illustrate the nearly linear behavior with dynamic pressure. Again, very little variation due to configuration is noted.

The repeatability of the repeat runs at η = 0.935 presented in figure 14 is shown in figure 20. The range of the repeat data is less than 0.06° with about 70% of the variation having a range of only 0.02°. Repeatability data for the 12 run pairs used for figures 15 – 18 for all 3 configurations are shown in figure 21. The mean of the differences between repeat runs is generally less than 0.02°. The maximum difference was generally less than 0.05° with a slight decrease in repeatability for the higher dynamic pressures. The maximum difference between repeat runs was less than 0.05° for 9 of the 12 run-pairs.

To summarize, the measured model deformation data showed detectable but generally small twist changes across the range of test conditions (Mach and dynamic pressures). The results of this measurement technique supported the evaluation of the force and moment results detailed in reference 9. There were no significant aeroelastic changes to the model with increasing dynamic pressure, and the data was not corrected for these minor effects.

Reynolds Number Effects

The effects of Reynolds number on the lateral-directional aerodynamics of this generic fighter configuration were analyzed for the three configurations and three different Mach numbers tested. Three angles of attack were investigated, for certain configurations and certain Mach numbers, to evaluate these effects for different flow states. These representative angles of attack were 1) α = 0 degrees, approximately minimum drag, 2) α = 6.0 degrees, a transitional flow state condition between attached flow and separated flow, and 3) α = 12.0 degrees, a separated flow condition. The highlights of this analysis are detailed below with key representative figures.

In addition, longitudinal data demonstrating the effects of fixing the boundary layer transition location for low Reynolds number conditions was analyzed. This data will show the effect of transition on the separate components of the configuration in detail and compare measured drag data to a theoretical estimate based on the variation of skin friction with Reynolds number.

Fuselage / Wing Configuration (FW) Lateral-Directional Rn Effects

For the baseline FW configuration, a minimum set of data over a small Reynolds number range was obtained as it was believed the most interesting results would be seen to with the introduction of the tailed configurations. For this configuration at a Mach number of 0.6, only two Reynolds number conditions were tested, Rn=5 and Rn=12 million; the results are shown in figure 22. No significant effect of Reynolds number on the stability derivatives is seen. It should be noted that the derivatives of

the yawing moment, side force, and rolling moment coefficients have been calculated between the range of −4 and +4 degrees sideslip, since the majority of the data was taken in this range. There was no further data taken at any other Mach numbers or Reynolds numbers for this configuration.

Fuselage / Wing / Centerline Vertical Tail / Horizontal Tail Configuration (FWV1H)
Lateral-Directional Rn Effects

The effect of Reynolds number on the single horizontal and single vertical tail configuration at a Mach number of 0.9 and two angles of attack are shown in figure 23. The characteristics of the directional stability show a general increase in stability with Reynolds number up to a moderate Reynolds number. For the lower angle of attack (α = 6 degrees), there is an initial increase (on the order of 20%) in the directional stability at a Reynolds number of 12 million and then no further effect is seen with increasing Reynolds number. For the higher angle of attack (α = 12 degrees), there is a similar characteristic of an increase in directional stability up to a Reynolds number of 22 million and then a destabilizing effect beyond this moderate Reynolds number. It appears the configuration is more sensitive to Reynolds numbers at higher angles of attack. The variations on the order of 20-25% could be significant, but do not, for instance, indicate any control reversals or major instabilities. There appear to be no significant effects of Reynolds number on roll stability characteristics which remain at a nearly constant level over the range of test conditions. Similar effects at Mach number of 0.6 and 0.9 have been observed and no drastic effects have been observed at these other flow conditions.

Fuselage / Wing / Trailing-Edge Extension / Twin Vertical Tail Configuration (FWTV2)
Lateral-Directional Rn Effects

The effect of Reynolds number on the twin–tailed configuration at a Mach number of 0.9 and two angles of attack are shown in figure 24. For this configuration, there is a gradual consistent decrease in directional stability, at an angle of attack of 6 degrees with increasing Reynolds number, on the order of 20-25% over the Rn range. For the higher angle of attack (α = 12 degrees), the effect of Reynolds number is much more abrupt with an initial decrease in stability, followed by a an increase, and then a sudden drop in the stability at the highest Reynolds number condition (Rn = 60 million). The higher angle of attack orientation in the separated flow regime appears much more sensitive to changes in flow conditions. The roll stability characteristics are similar to the previous configuration.

Boundary-Layer Transition Effects
Longitudinal Rn Effects

The initial wind tunnel test of the Pathfinder II model with the McDonnell Douglas defined wing (Test 77) was focused on a high Reynolds number database, and included only free transition for the entire range of Reynolds number conditions. There were no configurations tested that included a forced boundary layer transition as is typical of low Reynolds number testing in the NTF and conventional wind tunnel facilities. As documented in reference 9, the drag at zero lift for low and medium Reynolds numbers was found to be offset from fully-turbulent theoretical estimates based on skin friction theory. A systematic boundary-layer investigation was conducted that addressed the test technique of forced boundary layer transition. This approach involved the application, at low to medium Reynolds number (up to 12 million), of two types of roughness elements to force transition. The two types of roughness elements tested included the use of traditional carborundum grit and the more modern use of epoxy discs. Each component on the model (fuselage, wing, tails) was tripped to evaluate the effects of each component on the contribution to the offset from the fully-turbulent theoretical estimates. The baseline configuration results (no tail transition effects) will be presented but similar results were observed for the tailed configurations as well.

The first type of transition application tested was the traditional gritting strategy. The grit size selected was 180, based on critical roughness height estimates (ref. 13). For the fuselage transition, the transition was located 0.4" aft of the apex measured along the surface of the model. For the wing, the transition was located 0.2" aft of the leading-edge of the wing, measured perpendicular from the leading-edge. Figure 25 shows the results, at a Mach number of 0.9, of the component contributions to the

drag build-up and the comparison to fully-turbulent skin friction theory. The open symbols are the free transition configurations and the filled symbols are the fixed transition results. As can be seen, the effect of the nose transition on the zero lift drag results is about a 5 count drag increase as compared to the free transition results at Rn = 5 million. This indicates there is considerable laminar flow along the fuselage for the configuration when allowed to transition freely. The contribution of the wing by itself is approximately 15 counts of drag that indicates, once again, a considerable amount of laminar flow exists on the wing when the model is tested transition free. The combination of the wing and fuselage, tripped together, correspond to a 20 count drag increase and match well with the estimated fully-turbulent skin friction theory. The effects on the lift and pitching moment are negligible. Comparing the results at another Mach number, figure 26 shows the effect of the wing and fuselage tripped together at a Mach number of 0.8. Again, the contribution of the two components, tripped together, add up to about 20 counts of drag and compare very favorably with the fully-turbulent skin friction theory. As a reminder, this plot does not show the contributions of the wing and nose as isolated components (as in the previous plot) but only shows the effect of the combined two components tripped. The lift and pitching moment for this Mach number are also unaffected by the transition application. This would be expected for zero lift conditions. However, at transonic lifting conditions, this would not be expected due to shock/boundary-layer interactions.

A second type of transition trip, epoxy discs rather than grit, was also tested. The use of epoxy discs (small cylinders) has been the more preferred method of tripping the boundary-layer in wind tunnel facilities for a number of years. This method produces a more repeatable pattern as compared to the grit application. It is also believed, by some, to be a more repeatable and controlled test technique. Figure 27 shows a comparison of results from the application of epoxy discs to the baseline configuration at a Mach number of 0.8. The results are once again shown for the combined effect of the fuselage and wing transition, and not the isolated effects of each component. The combined effect of the transition corresponds to about an 18 count increase in drag. The results compare favorably with the theoretical, fully-turbulent estimate but do show a small difference with the grit technique. There again is no significant effect on the lift and pitching moment. The epoxy discs were placed at the identical positions on the wing (0.2" aft of leading-edge) and fuselage (0.4" aft of apex) as the grit transition and was sized based on the critical roughness height as before (ref. 13). The size of the discs was 0.0035".

From these results, we have quantified the consequences of expected laminar flow along the wing and fuselage at low Reynolds number if the boundary–layer is not tripped. It also indicates that the two components must be tripped together as a unit to produce the best low Reynolds number results from which to successfully scale drag as would be expected.

CONCLUDING REMARKS

Two wind tunnel tests of a generic fighter-type model were executed in the National Transonic Facility at NASA LaRC across a wide range of Reynolds numbers from that available in conventional wind tunnels to flight conditions at subsonic and transonic Mach numbers. General conclusions are summarized as follows:

1. Static aeroelastic effects on the longitudinal aerodynamic coefficients were detectable, but were generally small. The force and moment effects shown in reference 9 were verified with an improved video model deformation measurement system that measured the change in twist of wing under load during the latest model entry in the facility.
2. Reynolds number effects on directional stability over the angles of attack and sideslip investigated were significant, as changes on the order of 20-25% were observed over the Rn range tested. The effects appear to be more sensitive at higher angles of attack. Reynolds number effects on roll stability were small.
3. Zero lift drag for all Reynolds numbers scales with fully-turbulent skin friction theory. The standard technique of fixing the boundary layer transition location on the wing and fuselage at Reynolds numbers below approximately 22 million provides results in agreement with theory.

ACKNOWLEDGEMENTS

The authors would like to thank the Boeing Company, formerly McDonnell Douglas, for their support in this wind tunnel investigation. We would like to specifically thank Mr. Wayne L. Ely (retired) of McDonnell Douglas and Dr. Robert M. Hall of NASA LaRC for their important contributions before, during, and after these investigations. Without their efforts, these tests would not have been accomplished. Also, we would like to acknowledge the representatives of the National Transonic Facility for their support during the testing and subsequent data processing.

REFERENCES

1. Campbell, J.F.: "The National Transonic Facility – A Research Perspective," AIAA Paper 84-2150, August 1984.
2. Wahls, R.A.: "The National Transonic Facility: A Research Retrospective," AIAA Paper 01-0754, January 2001.
3. Luckring, J.M.: "An Overview of National Transonic Facility Investigations for High Performance Military Aerodynamics," AIAA Paper 01-0906, January 2001.
4. Ely, W.L.: "Summary Report for the Pathfinder II Full-Scale Reynolds Number National Transonic Facilty Wind Tunnel Test – Test 77," Report Number MDA 96P0049, October 1996.
5. Fuller, D.E.: "Guide for Users of the National Transonic Facility," NASA TM-83124, 1981.
6. Finley, T.D. and Tcheng, P.: "Model Attitude Measurements at NASA Langley Research Center," AIAA Paper 92-0763, 1992.
7. Foster, J.M. and Adcock, J.B.: "User's Guide for the National Transonic Facility Research Data System," NASA TM-110242, April 1996.
8. Wahls, R.A., Adcock, J.B., Witkowski, D.P., and Wright, F.L..: "A Longitudinal Aerodynamic Data Repeatability Study for a Commercial Transport Model in the National Transonic Facility," NASA TP-3522, August 1995.
9. Tomek, W.G., Hall, R.M., Wahls, R.A., Luckring, J.M., and Owens, L.R.: "Investigation of Reynolds Number Effects on a Generic Fighter Configuration in the National Transonic Facility," AIAA Paper 2002-0418, 2002.
10. Burner, A.W., Wahls, R.A., and Goad, W.K.: "Wing Twist Measurements at the National Transonic Facility," NASA TM-110229, February 1996.
11. Burner, A. W. and Liu, Tianshu, "Videogrammetric Model Deformation Measurement Technique. Journal of Aircraft", Vol. 38, No. 4, July-August, 2001, pp. 745-754.
12. Graves, S.S. and Burner, A.W., "Development of an Intelligent Videogrammetric Wind Tunnel Measurement System", SPIE's 46th Annual Meeting---The International Symposium on Optical Science and Technology, San Diego, California, July 29-August 3, 2001, Proc. SPIE Vol. 4448, Optical Diagnostics for Fluids, Solids, and Combustion, Carolyn R. Mercer; Soyoung S. Cha; Gongxin Shen; Eds, p. 120-131.
13. Braslow, A.L., and Knox, E.C.: "Simplified Method for Determination of Critical Height of Distributed Roughness Particles for Boundary-Layer Transition at Mach Numbers from 0 to 5," NACA TN-4363, 1958.

ref. area / NTF cross sectional area	0.023
model span / NTF width	0.211
solid blockage ratio, α = 0 deg	0.0039

Table 1. Model size relative to the NTF test section.

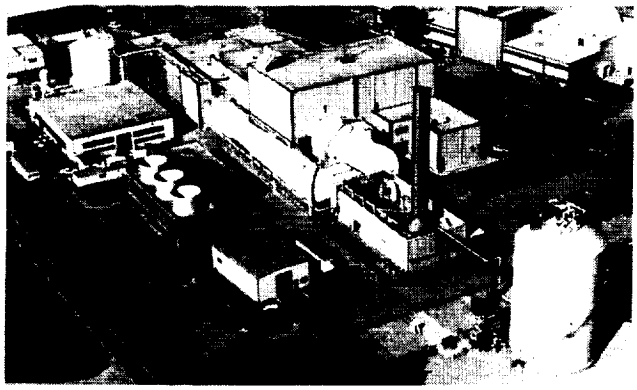

Figure 1. External view of the NTF.

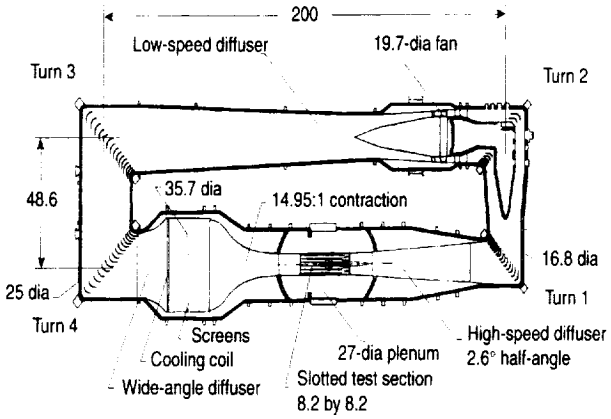

Figure 2. NTF circuit diagram (dimensions in ft).

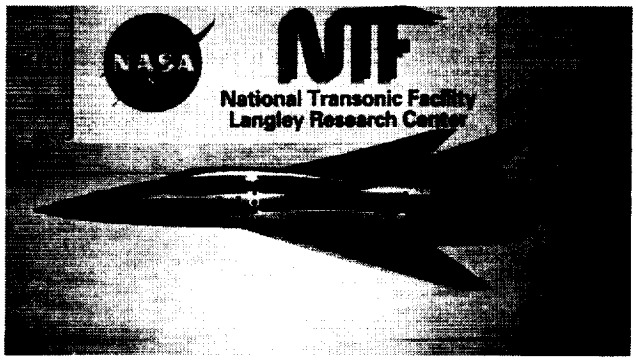

Figure 3. Pathfinder II model with McDonnell Douglas defined wing in the NTF.

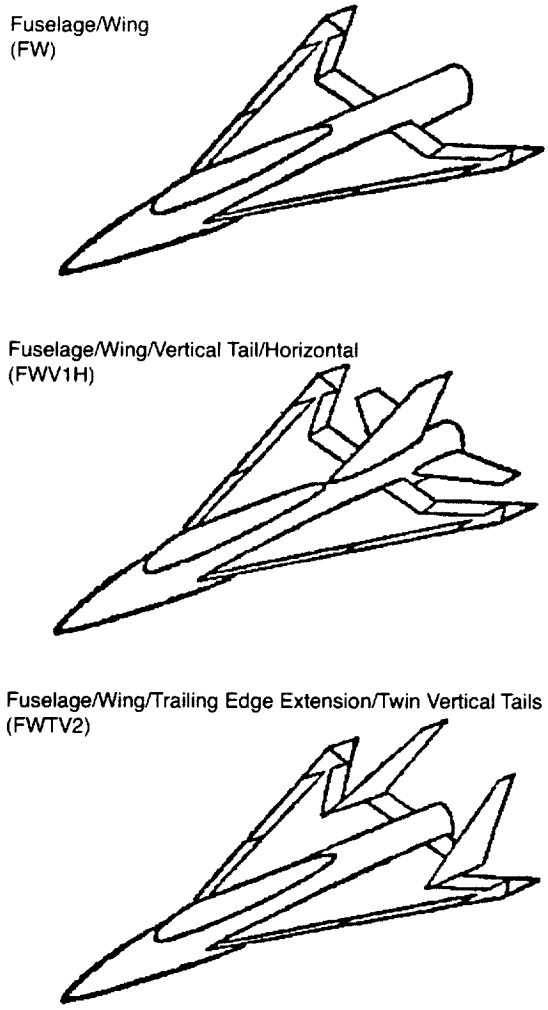

Figure 4. Pathfinder II model with McDonnell Douglas wing/empennage configurations.

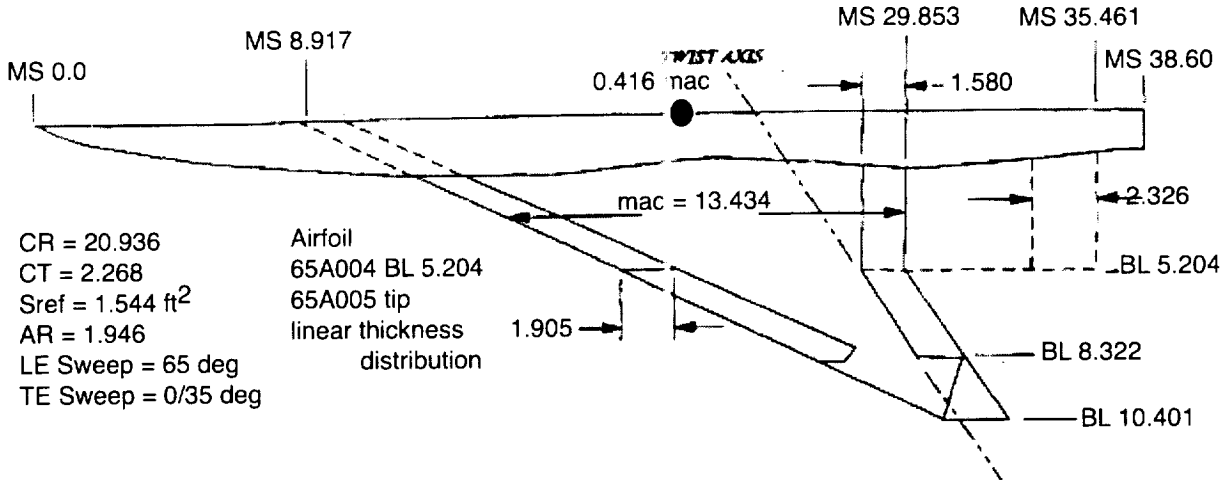

a) fuselage, wing, and trailing-edge extension (dimensions in inches).

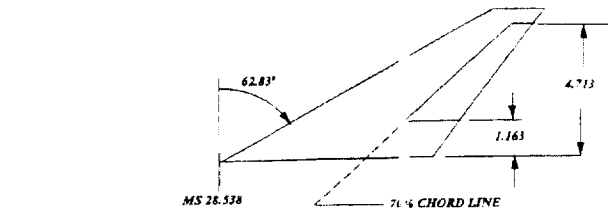

TWIN VERTICAL TAIL GEOMETRY
CR = 7.923 in
CT = 1.827 in
H = 5.236 in
S ref = 0.177 in²
S_{RUDDER} = 0.33 in²
AR = 1.07
Λ = 0.23°
CANT = 15° INBOARD

AIRFOIL SECTION
65A005
MODIFIED L.E. RADIUS = 0.159% c

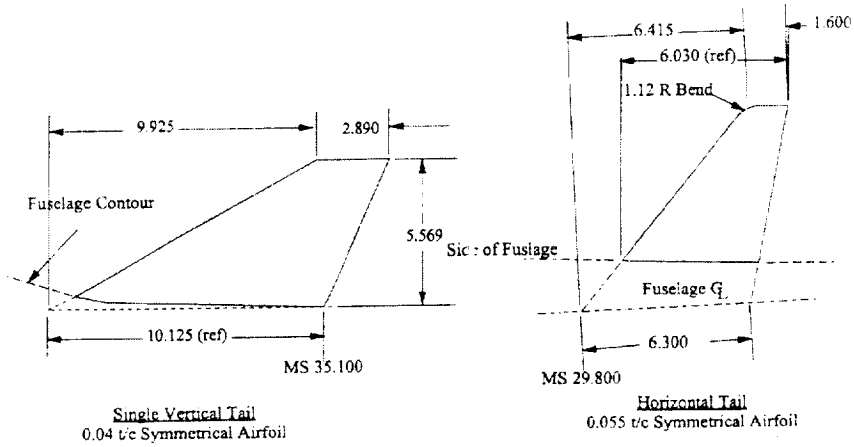

Single Vertical Tail
0.04 t/c Symmetrical Airfoil

Horizontal Tail
0.055 t/c Symmetrical Airfoil

b) empennage components (dimensions in inches).

Figure 5. Model geometry (dimensions in inches).

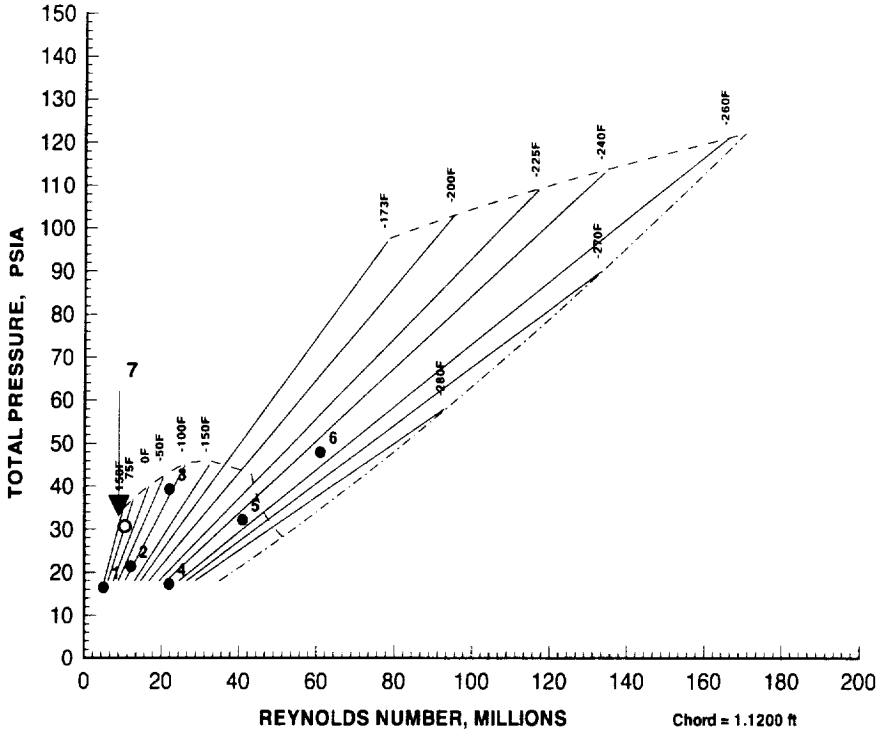

Figure 6. Test conditions, M = 0.90.

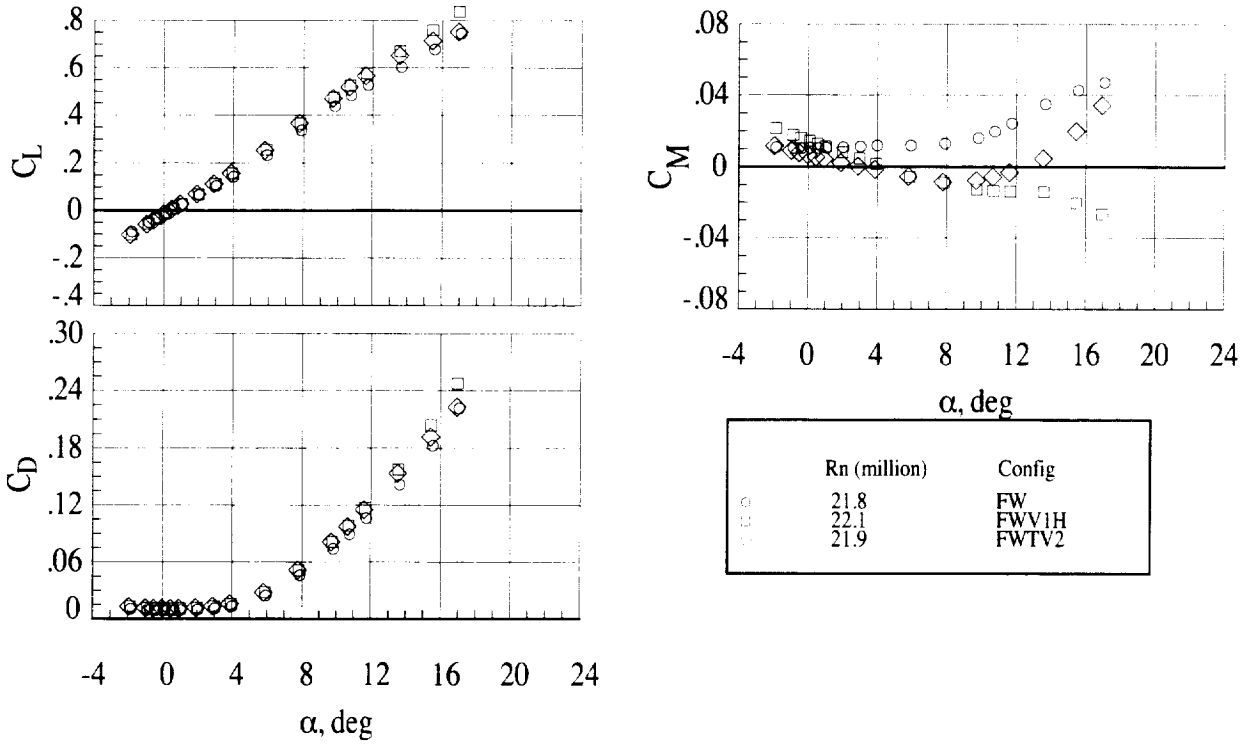

Figure 7. Representative longitudinal force and moment data, M=0.6.

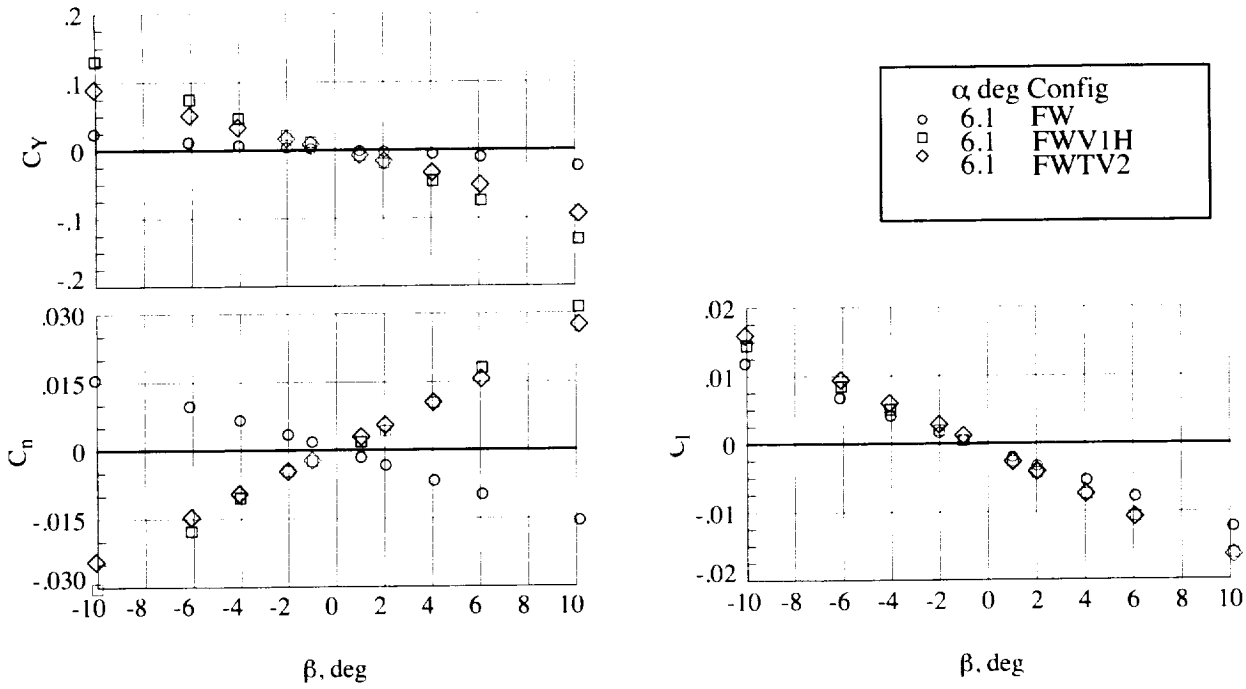

Figure 8. Representative lateral-directional force and moment data, M=0.6, Rn = 5 M.

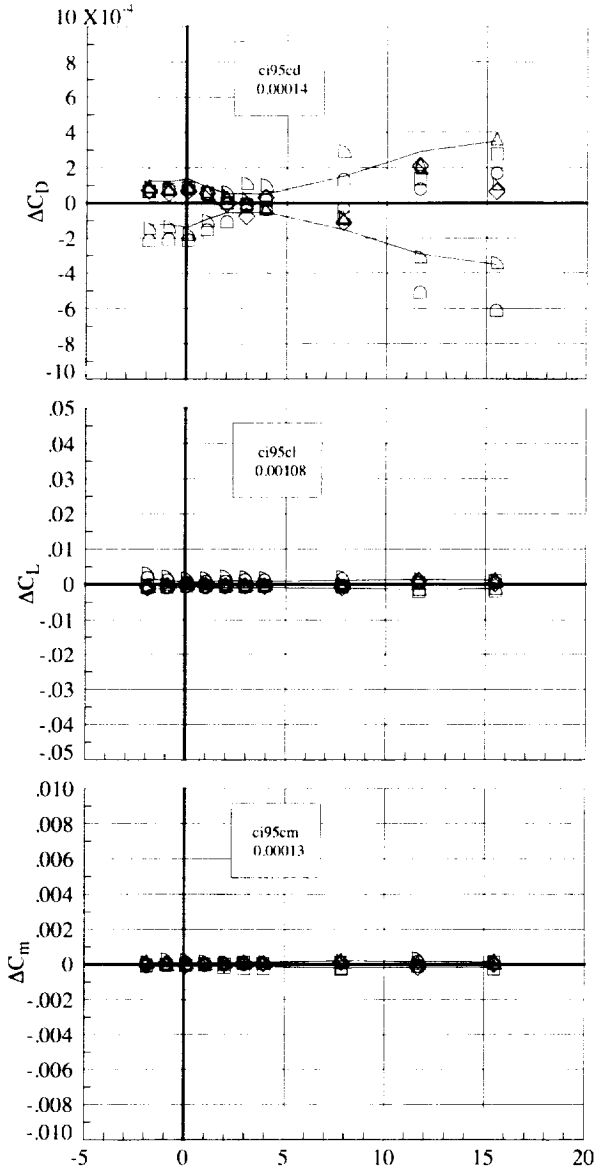

	Test	Rn (millions)	P_T, psi	T_T, F	q, psf
○	77	4.996	20.70	120.3	590.1
□	77	4.995	20.70	120.4	590.1
◇	77	4.995	20.70	120.4	590.1
△	77	4.995	20.70	120.4	590.1
▽	77	4.994	20.70	120.5	590.1
▷	140	4.977	20.70	121.8	589.5
◁	140	4.997	20.70	120.0	589.5

Figure 9. Long-term repeatability of longitudinal coefficients, FW configuration, M=0.6.

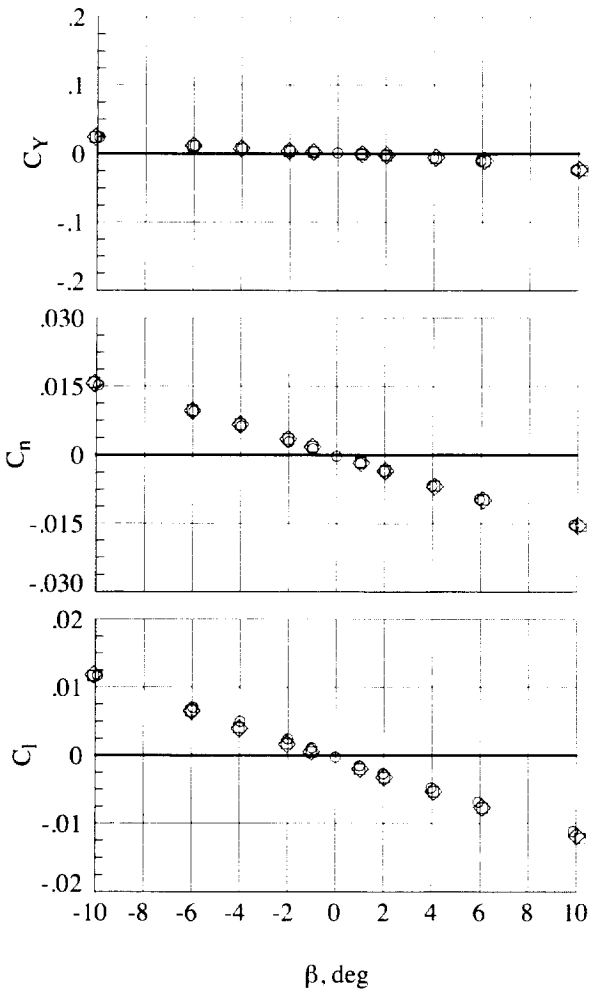

Test	Rn (millions)	α, deg
77	5.0	5.9
140	5.0	6.1
140	5.0	6.1

Figure 10. Long-term repeatability of lateral-directional coefficients, FW configuration, M=0.6.

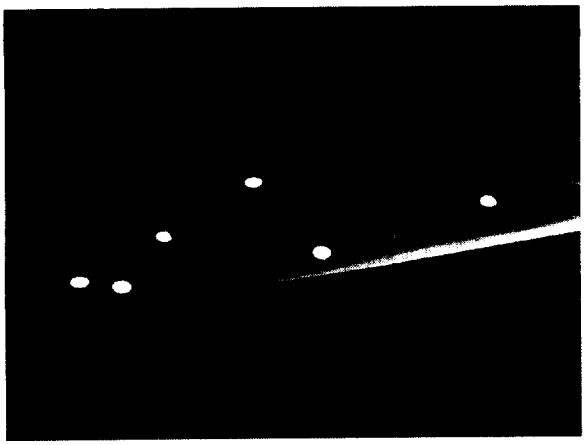

Figure 11. Image of right wing showing polished-paint targets at 3 semispan locations.

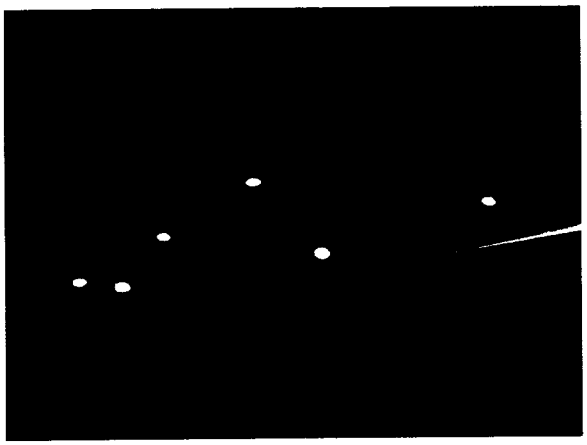

Figure 12. Raw image during data-taking illustrating high contrast.

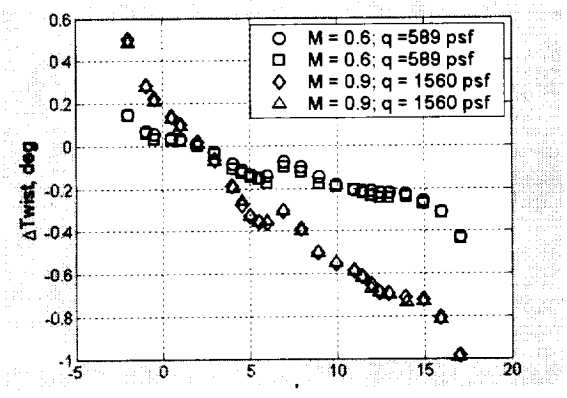

Figure 13. Aerodynamically induced change in twist with 5th order polynomial fits to reference polars. $\eta = 0.935$.

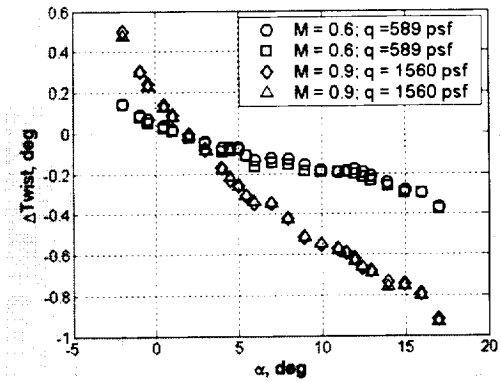

Figure 14. Aerodynamically induced change in twist with piecewise cubic Hermite interpolation fits to reference polars; $\eta = 0.935$

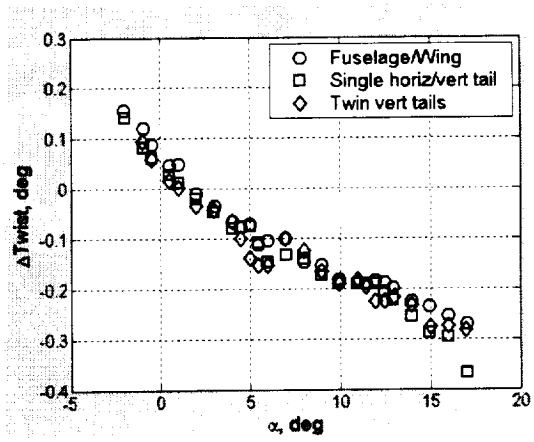

Figure 15. Aerodynamically induced change in twist at Mach = 0.6: q = 589 psf; $\eta = 0.935$

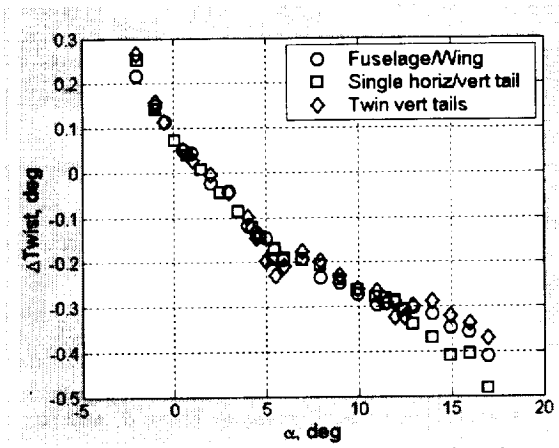

Figure 16. Aerodynamically induced change in twist at M=0.9;q = 797 psf; $\eta = 0.935$.

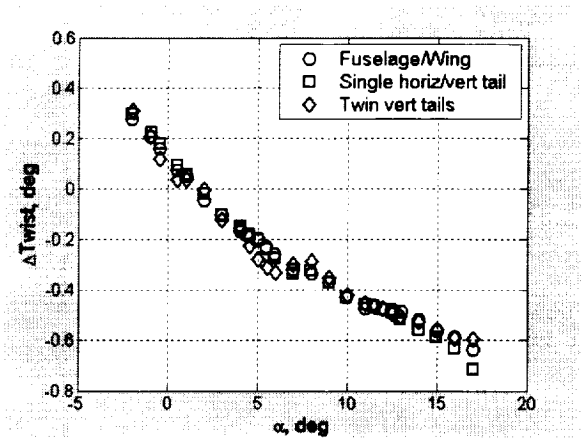

Figure 17. Aerodynamically induced change in twist at M = 0.6; q = 1415 psf; η = 0.935.

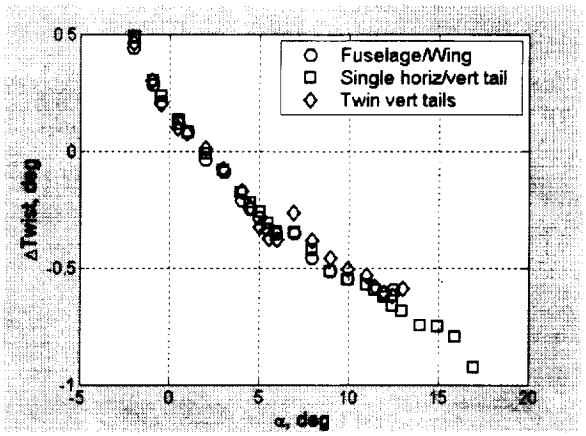

Figure 18. Aerodynamically induced change in twist at M = 0.9; q = 1560 psf; η = 0.935.

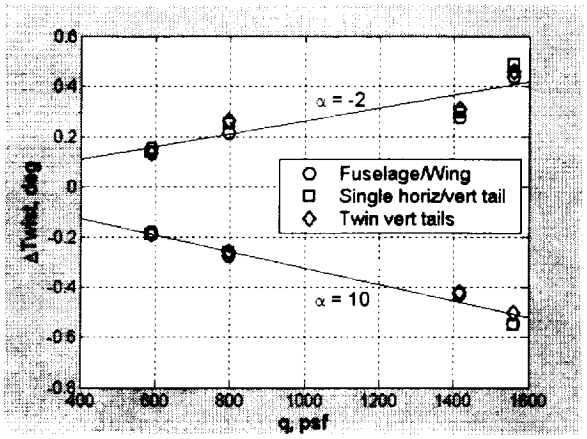

Figure 19. Aerodynamically induced change in twist versus dynamic pressure at α = -2° and 10°; η = 0.935.

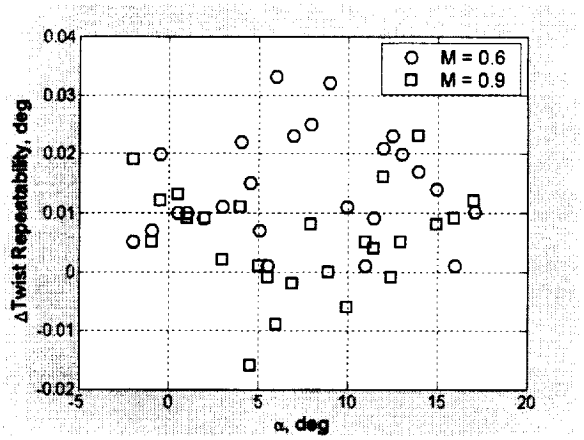

Figure 20. Repeatability of two nearly back-to-back runs versus α; η = 0.935.

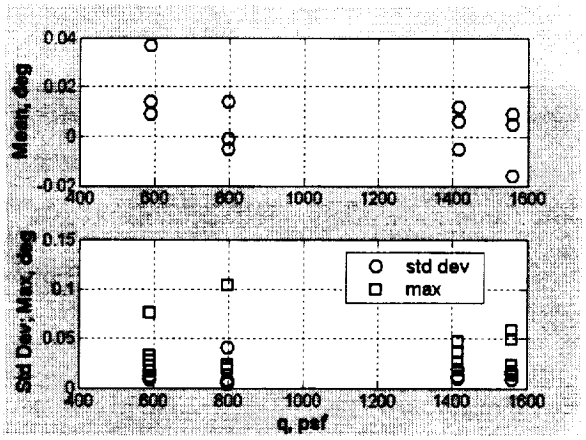

Figure 21. Repeatability of 12 run-pairs of nearly back-to-back runs versus dynamic pressure; η = 0.935.

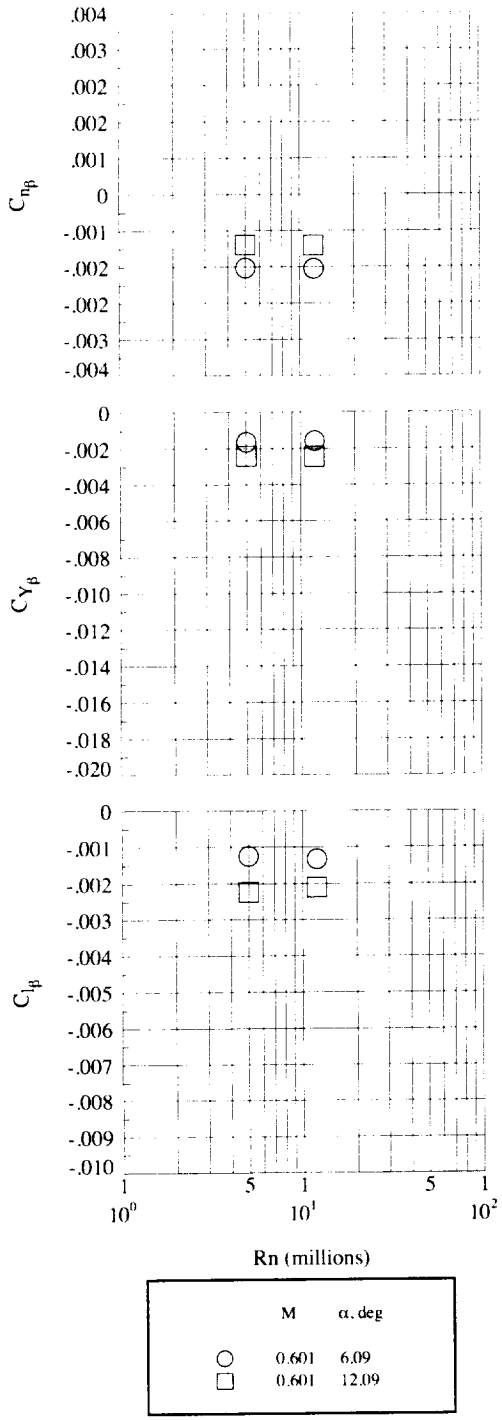

Figure 22. Lateral-directional stability trends with Reynolds number, FW configuration, M=0.6.

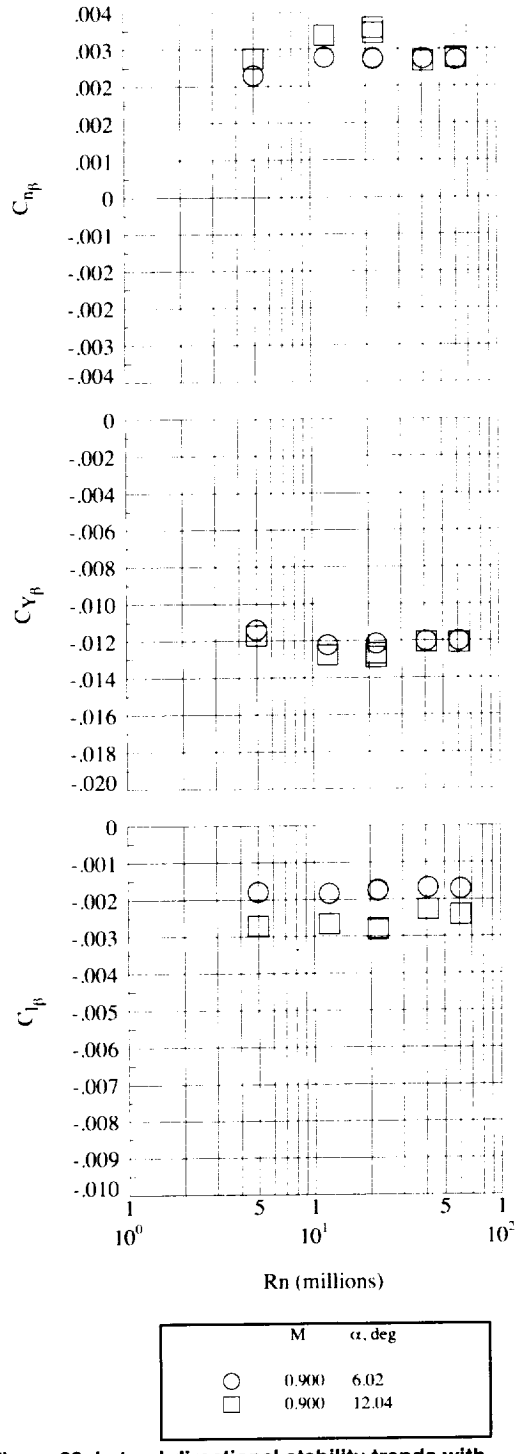

Figure 23. Lateral-directional stability trends with Reynolds number, FWV1H configuration, M=0.9.

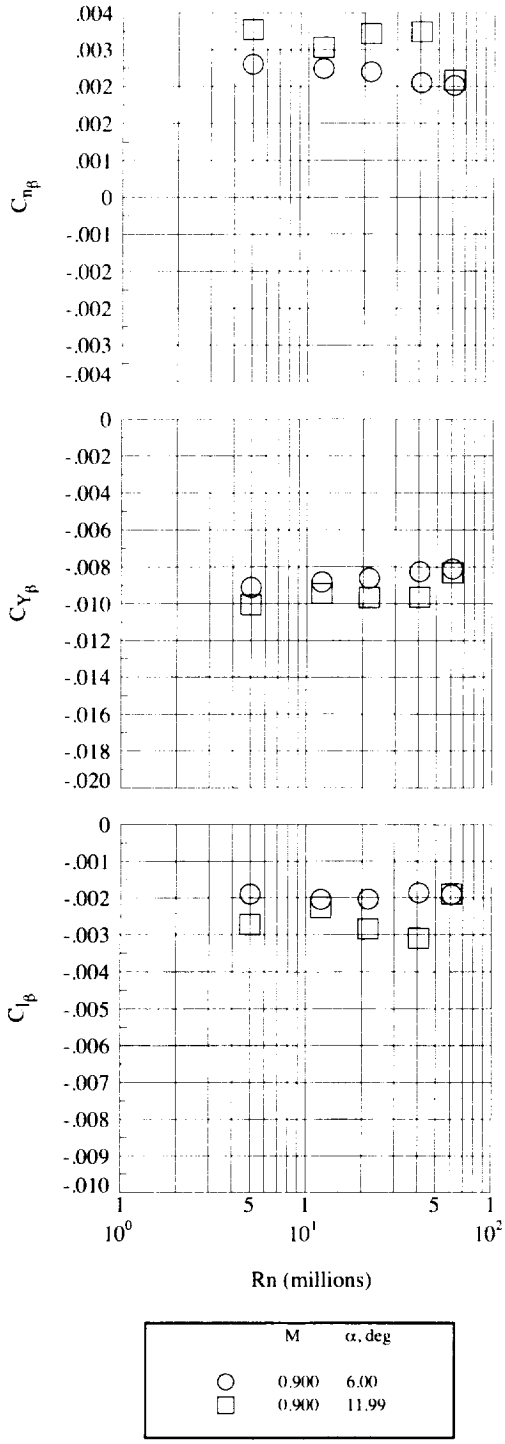

Figure 24. Lateral-directional stability trends with Reynolds number, FWTV2 configuration, M=0.9.

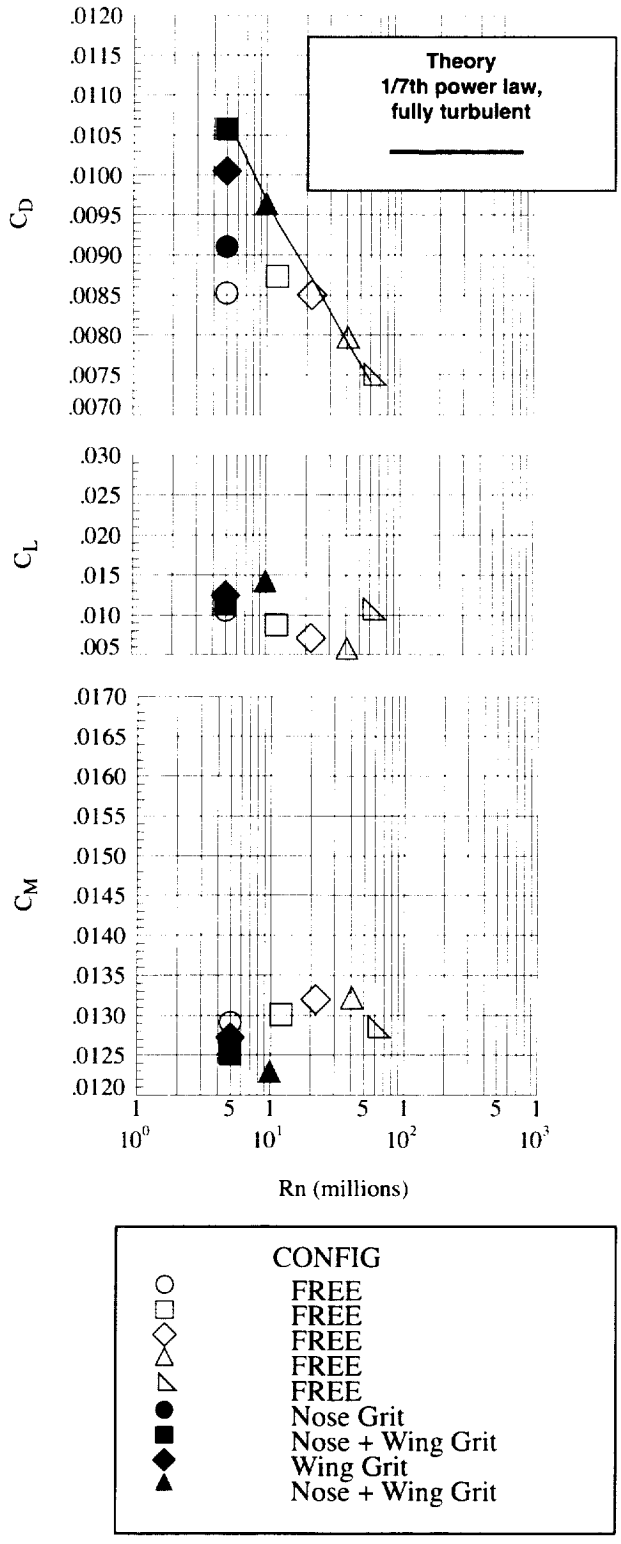

Figure 25. Longitudinal coefficient trends with Reynolds number, FW configuration, near minimum drag, M=0.9.

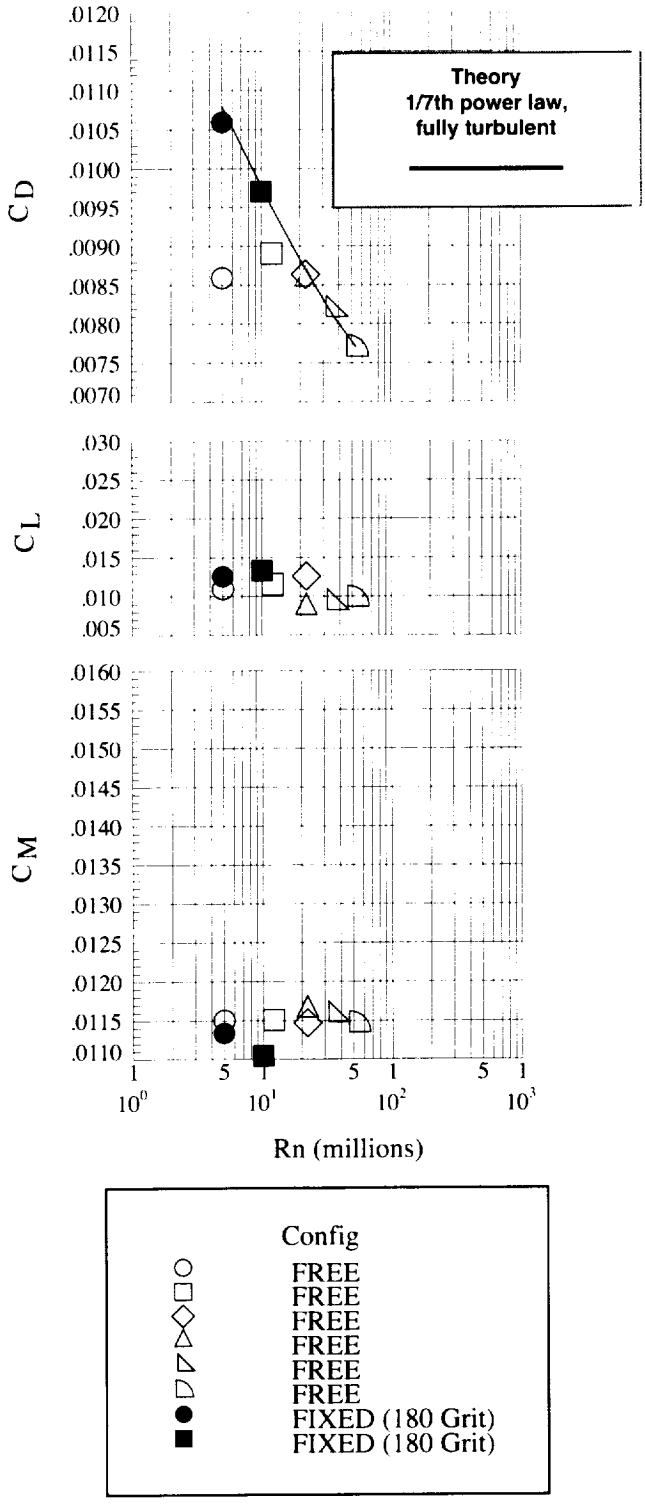

Figure 26. Longitudinal coefficient trends with Reynolds number, FW configuration, near minimum drag, M=0.8.

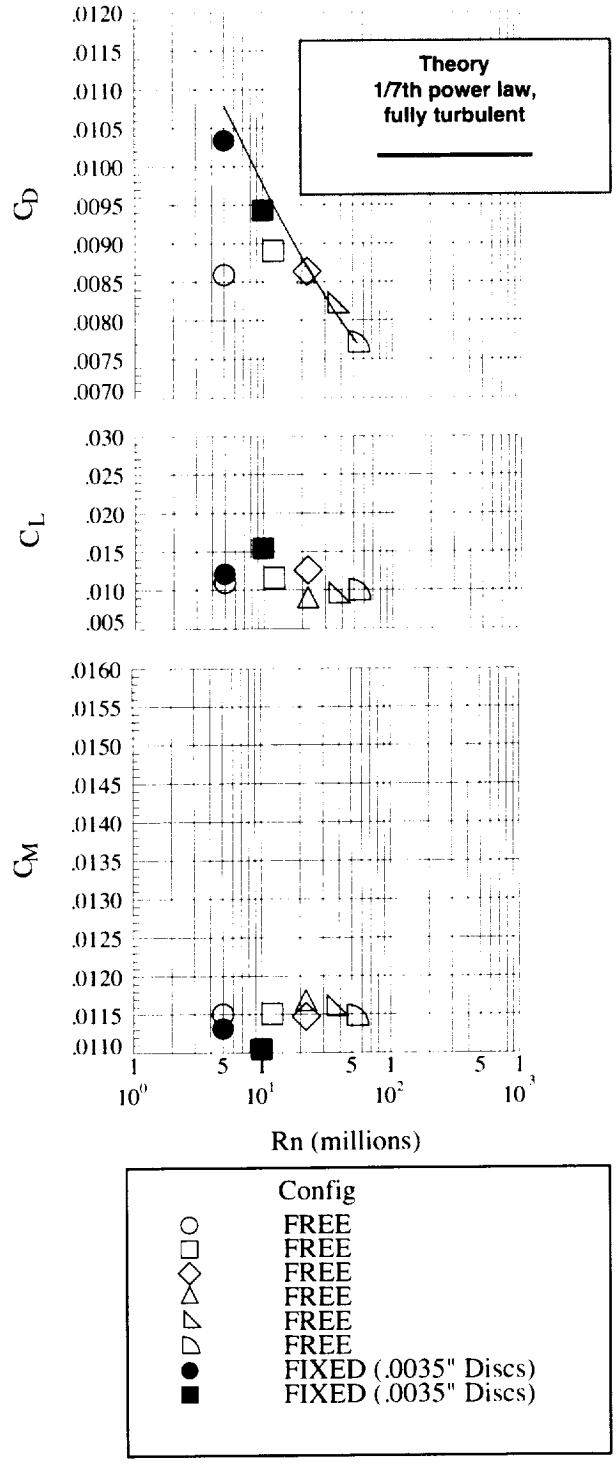

Figure 27. Longitudinal coefficient trends with Reynolds number, FW configuration, near minimum drag, M=0.8.